Journal of Manufacturing Systems 83 (2025) 963–975

Contents lists available at ScienceDirect

Journal of Manufacturing Systems

journal homepage: www.elsevier.com/locate/jmansys

Technical paper

Efficient human–robot collaborative manipulation of planar deformable objects

Enrico Villagrossi [a,*], Paolo Franceschi [b], Giorgio Nicola [b], Nicola Pedrocchi [a]

[a] Institute of Intelligent Industrial Technologies and Systems for Advanced Manufacturing (STIIMA) - National Research Council of Italy (CNR), Via A. Corti, 12, Milan, 20133, Italy

[b] Department of Innovative Technologies, University of Applied Science and Arts of Southern Switzerland (SUPSI), Via la Santa 1, Lugano, 6962, Switzerland

ARTICLE INFO

Keywords:
Human–robot collaborative transportation
Planar deformable object collaborative transportation
Physical Human-Robot Interaction (pHRI)
Planar deformable object deformation estimation

ABSTRACT

This paper presents an efficient method to improve the productivity and the accuracy of human–robot collaboration in transporting large, planar, deformable objects, specifically during the production of parts made of advanced composite materials. The proposed approach utilises an industrial robot to assist operators in transporting and handling carbon fibre and fibreglass plies during draping. A consumer vision system feeds a data-driven model that estimates the material's deformation from depth images. This deformation data, transformed into force/torque information via a virtual spring, informs a Human–Robot Role Arbitration (RA) algorithm that dynamically adjusts leadership between humans and robots based on context, enhancing safety and efficiency. Inspired by game theory, the approach adapts to cooperative and non-cooperative scenarios, demonstrating significant productivity gains over traditional algorithms used for the same scope. The paper also compares the use of the RA algorithms with the current industrial practice, which relies entirely on manual production. Company operators, working in a production site, performed the experimental comparison producing a real boat propeller.

1. Introduction

Strategic sectors like aerospace, automotive, and maritime rely on advanced composite materials, often using large fabric plies made from carbon fibre or fibreglass for structural parts. Production typically involves small batches or unique components, particularly in the space industry, which limits full automation. As a result, manual labour and artisan skills are essential [1]. Robotics can enhance flexibility by assisting operators in manipulating and positioning these bulky plies [2], ensuring accuracy while maintaining human supervision to avoid errors that could impact the final product's mechanical properties. Despite the great potential of robotics in this application, unaddressed issues remain. The robot should know the object's path or final position through signals from the human operator or haptic communication via the co-manipulated object. However, manipulating fabric-like objects (an example of a planar deformable element) can limit haptic feedback since the material's mechanical properties may prevent standard robot end-effector sensors from measuring all applied deformations as force/torque. Second, the robot should share the workload with the human while allowing for control exchange, enabling continuous shifts in leader and follower roles [3]. Finally, an issue in manipulating bulky objects is the rotation–translation ambiguity encountered in human–robot [4] and human–human [5] collaborative applications.

The contribution given in this work is fusing the methods proposed in [6] and in [7] to achieve a reliable robotic application for the human–robot collaborative transport of fabric-like objects. Specifically, [7] proposed a human–robot RA based on game theory, tested on rigid materials and using a Force/Torque (F/T) sensor to measure the interaction force. In [6], the authors proposed an indirect measure of the human intention during the interaction by capturing images of the bent object during the manipulation and adjusting the robot's path accordingly. The paper used a Deep Learning algorithm to estimate the material deformation. Such a method also allows manual guidance in manipulating objects, avoiding any compression strength.

The effectiveness of the fusion of [6,7] has been proven in a real industrial use case scenario from a company active in composite material parts production (draping[1] of a sports car hood and spoiler). Experiments with seven users involved in a human–robot collaborative transport of a carbon fibre ply demonstrated performance improvements in productivity and accuracy compared to a state-of-the-art

* Corresponding author.
E-mail address: enrico.villagrossi@cnr.it (E. Villagrossi).

[1] draping is the process of placing layers of carbon fibre fabric in a mould. During this process, the flat fabric distorts to fit the shape of the mould.

https://doi.org/10.1016/j.jmsy.2025.11.011
Received 14 April 2025; Received in revised form 15 October 2025; Accepted 11 November 2025
Available online 19 November 2025

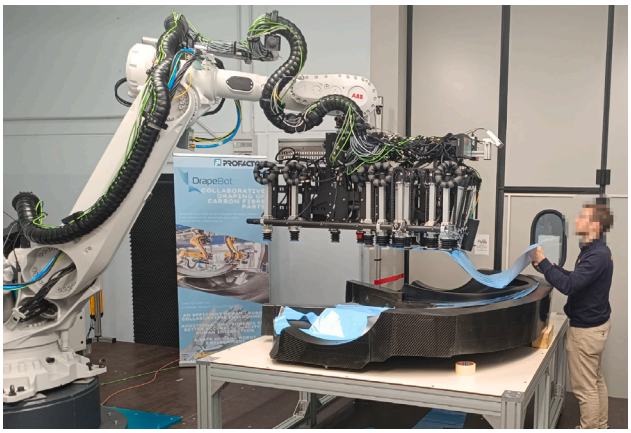

Fig. 1. Example of human–robot collaborative transport of a carbon fibre ply.

method. Using the proposed method also brought a more repeatable process in terms of execution time with a consequent lower variance in cycle time. In addition, the paper compared the proposed approach with a completely manual task (as is the current industrial production process) of producing a boat propeller; in this case, the process required the draping of 70 plies involving three company operators without specific robotic knowledge. Experiments demonstrated that using the robot for collaborative transport brought higher production time but reduced the cycle time variance. Using a more mature robotic system can reduce the number of operators (*i.e.,* using the robot as an added operator) with the benefits of a more repeatable and traceable process, which can justify higher production time and the higher cost of the equipment.

Our method can easily extend to other fabric-like materials (*e.g.,* clothing, composite fibres, wrapping materials) and semi-rigid objects (*e.g.,* thin foam panels, rubber sheets) and supports operators in positioning with extreme precision large carbon fibre plies from picking table into a mould during the draping process, still letting the human lead the task in most situations. The dimensions of transported plies motivate the use of two agents (*i.e.,* the human and the robot), as in Fig. 1. Humans and robots also have complementary capabilities, such as human supervision and reasoning capacity, combined with the robot's repeatability and accuracy.

The paper is organised as follows: Section 2 analyses the related works; Section 3 illustrates the theoretical approach; Section 4 describes the use case and the experimental setup; Section 5 presents evaluation indices to measure the framework's performance and discusses the results obtained during the experimental sessions; Section 6 compare the collaborative framework with the manual process during the collaborative transport. Finally, Section 7 reports the conclusions and the future works.

2. Related works

Using robotics to manipulate deformable objects in industrial applications is growing [2]. The literature presents several works on the topics with a vast variety of applications of different kinds of objects treated [8]. The manipulation of fabric-like objects resolves around folding fabric [9,10], mostly with applications in the fashion industry. Other examples of fabric manipulation with robots involve advanced composite materials as in [11,12], where robotics is still pioneering. There is still a limited focus on studying robot–robot [13] and human–robot collaborative transport of fabric-like objects [14].

The human–robot collaborative transport of bulky fabric-like objects has great potential for application in producing advanced composite materials [15,16]. This approach exemplifies the Industry 5.0 paradigm [17], enabling human-centric production where humans focus on higher-value tasks while robots provide support. In the literature, human–robot collaborative transport is mainly dedicated to rigid objects exploiting force-based algorithms implementing what is also known as *manual guidance* control where the human guides the robot directly applying forces (measured with F/T sensors) on the robot itself or through the manipulated object [18]. This approach fails with non-rigid objects since force torque measurements are unreliable. The human–robot transportation problem of fabric-like objects is poorly studied; currently, two main approaches have emerged for this scenario: human motion capture and direct deformation estimation of material. The most common method consists of capturing human motion during the collaborative transport (*i.e.,* skeleton tracking) with vision systems [16,19,20] or IMU-based sensors [21] combined with F/T sensors to feed impedance/admittance control algorithms. In the case of human motion capture, with either IMU sensors [22] or cameras [19,20,23,24], the positions of points where the material is grasped by both the robot and the human are tracked. Tracking these points assumes that their positions on the manipulated object are known beforehand or detectable. This enables the reconstruction of the material's shape using physics simulation software [19,25]. Otherwise, the relative distance between the human and the robot is used as input to the controller [22]. Differently in [26], material deformation was estimated using a camera (RGB-D camera) to detect visual features (*i.e.,* deformation w.r.t. a rest position) on the manipulated material, which are then converted into robot commands, avoiding the human position tracking. In [24], the authors introduced a motion planner, able to respect safety limits, while planning robot trajectories in real-time. The aim is to track human and robot movements during the collaborative transport and plan the robot trajectory accordingly to human movements.

In every physical Human–Robot Interaction (pHRI) application, a crucial aspect is defining the role of the two actors, the robot and the human. Indeed, it is typical that one leads the action while the other follows, possibly assisting. The robot leading the task is typically used for clinical and rehabilitation applications [27,28]. On the contrary, the robot is typically a follower providing assistance and empowerment to the human in manufacturing applications such as load reduction during manual guidance [29,30]. Among others, Game-Theory is an increasingly prevalent trend in literature to model the interaction with a focus on the pHRI. The concept of Nash Equilibrium (NE) is utilised in [31] and similarly in [32], where NE updates the robot's cost function based on the interaction force exchanged with the human. This differential non-cooperative Game-Theoretic (GT) modelling approach is adopted in [33,34], employing policy iteration to update the robot's cost function like the previous works. An extension to these works is [35], which addresses the trajectory tracking problem within a non-cooperative scenario. Finally, [3] explores the cooperative scenario, where the weighting factor is adjusted variably to facilitate the adaptive impedance behaviour of the robot.

At the EU level, several research initiatives have been put in place. The EU H2020 projects Merging [36] and DrapeBot [37] are pioneering actions coping with these challenges in the industrial scenario. The project Merging looks at the manipulation of soft and fragile objects, exploiting multiple industrial robots, designing new Electro-Adhesive (EA) grasping devices, using information from perception systems fused with the data from a digital twin to estimate the deformations of soft elements [19,38]. The DrapeBot project focuses on the robotic manipulation of carbon fibre and fibreglass plies during the draping process; in particular, the work [39] highlights the importance of the human–robot manipulation when the dimension of the ply requires more than one robot.

3. Methodology

We address the collaborative transport of planar deformable objects through a general framework, as illustrated in Fig. 2. For the sake of

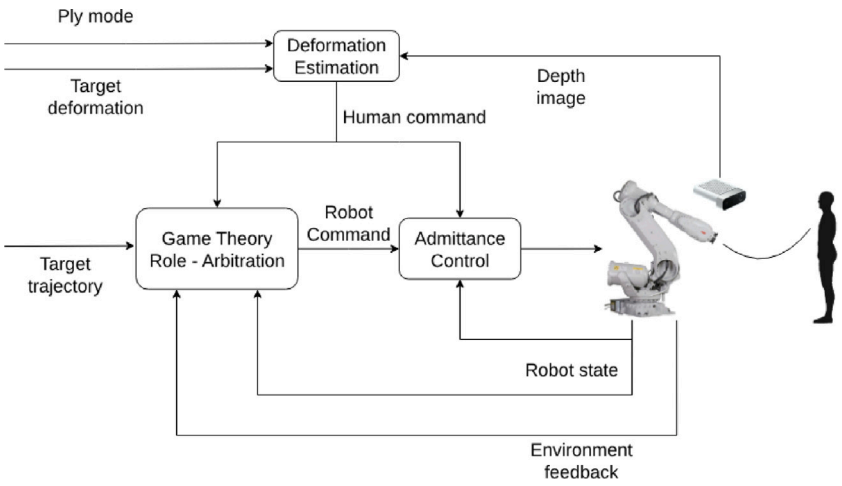

Fig. 2. Control scheme of the collaborative transport framework.

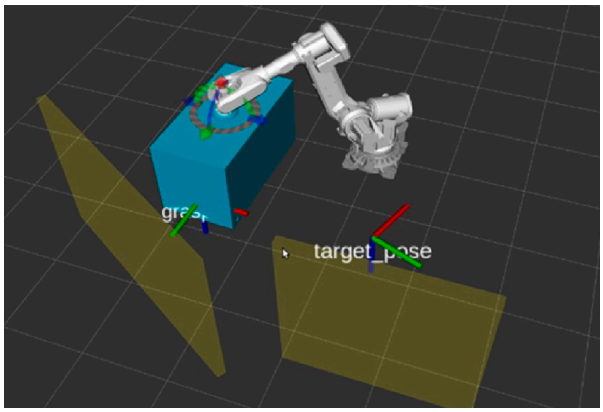

Fig. 3. The robotic cell and its boundaries are defined as collision objects in yellow; the gripper is highlighted in blue. (For interpretation of the references to colour in this figure legend, the reader is referred to the web version of this article.)

clarity, Fig. 2 is a simplified version with only high-level components; for the detailed control scheme, refer to Fig. 18 in Appendix. The control framework is based on two main elements: the role arbitration and the deformation estimation modules. The first module is grounded on a manual guidance control architecture enhanced with game theory, as investigated in [7], allowing dynamic role exchange between humans and robots to optimise performance and minimise risks like collisions. The second module involves material deformation estimation, utilising methods from the previous studies [6,40]. This process starts with raw depth images to assess the current deformation of a deformable object. The comparison to a desired setpoint reflects the human–robot distance from a rest position. Virtual springs were used to turn the deformation into a force input for the admittance control, used for the robot guidance control.

3.1. Role arbitration

With RA we refer to the mechanism that assigns the role of leader/follower to the robot, according to the situation and the human intentions. Given the theoretical approach introduced in [7], we want to design a law that allows the robot to be as assistive as possible when the human is leading the task far from undesired situations while taking control if the human is approaching dangerous situations. Moreover, we want the robot to reach the target position with extreme precision for manufacturing constraints. Therefore, the robot must also take the lead when approaching the target pose. For $\alpha > 0.5$ the robot is assistive, and the Cooperative interaction is considered (see [3] for the definition of α). The RA law objective is to define the parameter α to achieve this behaviour. For $\alpha < 0.5$ the Non-Cooperative interaction model is active, and the robot strictly tends to follow its own goal. The value $\alpha = 0.5$ determines the transition between the Cooperative and the Non-Cooperative interaction model. The shifting of α from 1 to 0 determines the modification of the two model parameters to enable a smooth transition between them when $\alpha = 0.5$. In this sense, for values of $\alpha \approx 1$, the robot behaviour tends to be assistive and follower, while for values of $\alpha \approx 0$, the robot takes the lead.

In general, undesired situations refer to (i) proximity to joint limits, (ii) low manipulability and singularities, (iii) proximity to obstacles, and (iv) proximity to workspace boundaries. Industrial workcells should be designed to avoid most of the undesired situations related to bad joint configurations [41], and the arbitration law can be reduced to obstacle avoidance and proximity to the target pose. We define two indices that measure the distance from obstacles and target pose. Note that this simplified formulation can consider any undesired Cartesian position, including workspace boundaries, a virtual collision object. The distance from the object index is computed as

$$d_o = \min(robot - objects). \tag{1}$$

The distance to the reference target position d_{trg} is measured as the Euclidean distance between the current end-effector position and the target position of the task (*e.g.,* pick/place pose)

$$d_{trg} = \left\| x^{ee} - x^{trg} \right\|, \tag{2}$$

with $x^{trg} \in \mathbb{R}^3$ denoting the target position and $x^{ee} \in \mathbb{R}^3$ denoting the end-effector position. The RA law, in the end, measures the distance from target d_{trg} as in (2), and the distance from collisions (real and virtual) d_o as in (1). A sigmoid function modulates the two values to obtain $\alpha_{trg} = \sigma(d_{trg})$, and $\alpha_o = \sigma(d_o)$, with σ denoting the sigmoid function. Finally, the parameter α is obtained as

$$\alpha = \min(\alpha_{trg}, \alpha_o). \tag{3}$$

Note that this is not the only possible choice of α. The selection of the minimum is the most conservative choice over the considered situations. Another option could be a weighted sum of the two values. The interaction model and its solution are selected according to the value of α. An explicative robotic cell is visible in Fig. 3; the yellow walls represent the workspace boundaries as collision objects, while the robot gripper is highlighted in blue. Further details on RA, GT modelling and the control framework are reported in Appendix.

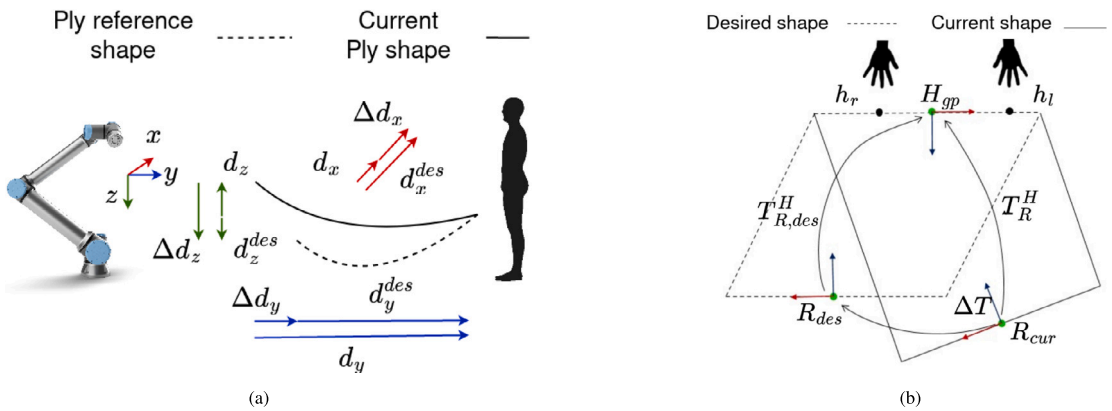

Fig. 4. Human–robot collaborative transportation. (a) Lateral view, highlighting the parameters that compose $T_R^H \in \mathbb{R}^{4\times4}$, $T_{R,des}^H \in \mathbb{R}^{4\times4}$, and ΔT. For the sake of simplicity, rotations have been neglected. (b) Top view, highlighting the definition of the human grasping point $H_{gp} \in \mathbb{R}^3$.

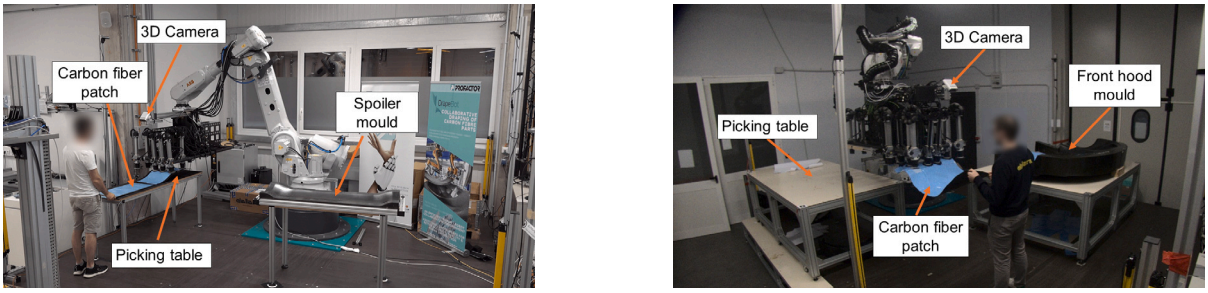

Fig. 5. Layout of uses cases. (a) Use Case 1 (UC1) to manufacture the Dallara "La Stradale" spoiler. (b) Use Case 2 (UC2) for the manufacturing of the Dallara "La Stradale" front hood.

3.2. Deformation estimation

This section briefly describes the deformation estimation problem in collaborative manipulation applications and the solution developed in [6,40]. For the sake of brevity, only the theoretical background is described. For a deeper analysis, we refer to [6,40].

Consider a deformable material handled by two agents, a human and a robot, shown in Fig. 4(a). Denote $h_r \in \mathbb{R}^3$ and $h_l \in \mathbb{R}^3$ as the human's right and left hand grasping positions and $R_{cur} \in \mathbb{R}^3$ as the robot's current grasping point. It was assumed that humans do not deform objects between their hands, for example, by spreading their arms. Thus, the human grasping point can be described with a single arbitrary point $H_{gp} \in \mathbb{R}^3$ between h_l and h_r. The object shape can be described by the relative roto-translation, defined with the homogeneous transformation matrix $T_R^H \in \mathbb{R}^{4\times4}$, between the robot grasping position R_{cur} and the human holding position H_{gp}. Therefore, the desired shape can be similarly described as the relative roto-translation, defined with the homogeneous transformation matrix $T_{R,des}^H \in \mathbb{R}^{4\times4}$, between the robot desired grasping position R_{des} and the human holding position H_{gp}. T_R^H and $T_{R,des}^H$ are respectively described by the parameters $d_R^H \in \mathbb{R}^6$ and $d_{R,des}^H \in \mathbb{R}^6$, three translations and three rotations following the X–Y–Z extrinsic Euler convention. T_R^H is unknown. Thus, the estimated roto-translation $\hat{T}_R^H \in \mathbb{R}^{4\times4}$ is defined. It can also be described by $\hat{d}_R^H \in \mathbb{R}^6$.

A deep learning-based deformation model processes depth images from an RGB-D camera on a robotic gripper to estimate $\hat{d}_R^H$. This deformation model, built on Densenet-121 and trained on various objects in the dataset, has a common backbone and a specialised last layer for improved transferability. The deformation model takes segmented depth images as input. The segmentation process to remove the background and the person is achieved via a deep learning segmentation model based on Unet that was fine-tuned on the same dataset.

3.3. Virtual wrench and human target estimation

Previous work in [7] relies on force exchange between humans and robots, measured through the force–torque sensor. As a fabric-like object that can only transfer traction forces, these forces can be applied when the fabric is fully extended and under tension, with a real risk of damaging the material if excessive force is applied. To overcome this issue, a method to estimate a virtual exchanged force $\hat{u}_h \in \mathbb{R}^6$ was defined based on the measure of material deformation explained in Section 3.2. It was defined as a nominal desired distance between the human hands and the robot tool, lower than the maximum allowed by the material. That distance, called $d_{R,des}^H \in \mathbb{R}^6$, represents the resting distance of the material, which gives the zero-wrench state. This implies that the ply, during the co-manipulation, must always be without tension. Otherwise, the ply deformation will always be the same for any applied force. Therefore, any deformation for such a position is defined by the estimated distance between the human and the robot $\hat{d}_R^H \in \mathbb{R}^6$. The difference $\Delta d = \hat{d}_R^H - d_{R,des}^H$ is the deformation directly related to the force the human imposes on the system. Since typically wrenches have magnitudes different from the deformations allowed by the co-manipulated plies, the relative distances are multiplied by a vector of gains $K_d \in \mathbb{R}^6$ to convert them into wrenches, resulting in

$$\hat{u}_h = K_d \odot \Delta d. \tag{4}$$

The values of K_d are experimentally identified to let the virtual wrenches lie in ranges similar to the ones measured via force/torque sensors in classical pHRI tasks. In this way, it is possible to tune the controller's parameters with similar values for both rigid and flexible objects.

Finally, given the human virtual force, it is necessary to identify the human reference trajectory $\hat{x}_{h,ref} \in \mathbb{R}^6$ to feed the RA algorithm (see Fig. 18). Several methods and works investigate this topic [42–46],

implementing complex models whose design and training require a lot of data. This work defined it as an easy yet powerful update law for the desired human motion. The desired human intention of motion $\hat{x}_{h,ref}$ is updated at each cycle by the following

$$\hat{x}^{t}_{h,ref} = x^{t-1}_{h,ref} + K_{p,h}\,\hat{u}_h \tag{5}$$

with $\hat{x}^{t}_{h,ref}$ and $x^{t-1}_{h,ref}$ referring to the updated and previous poses, respectively, and $K_{p,h}$ defines a coefficient proportional to the human exerted virtual force.[2]

4. Industrial use cases and setup

The proposed framework was tested on two similar use cases derived from the automotive industry, specifically the manufacturing of the spoiler, namely Use Case 1 (UC1) see Fig. 5(a), and the front hood, namely Use Case 2 (UC2) see Fig. 5(b) of the Dallara "La Stradale" sports car. A third use case (UC3) will be presented in Section 6. UC3 involves the production of a boat propeller. The control framework and the setup presented in this work will be compared with a manual production process.

The spoiler and front hood are made from pre-preg carbon fibre, layered into plies with complex shapes. Currently, operators manually layup and drape the plies in the mould, with larger ones requiring multiple operators. The proposed framework facilitates the collaborative transport of large plies from a picking table, where they are identified by a vision system, allowing for random placement and high repeatability in picking.

The UC1 and UC2 present complementary challenges that the proposed framework can address. In UC1, transporting the ply near the mould is difficult due to a 90-degree turn near the robot's workspace limit and safety fences. The gripper holds the ply by its edge, and two issues arise. First, the back of the gripper is in a blind spot from the operator's point of view. Second, the distance between the human and the back of the gripper is considerable, leading to significant movements in the gripper's back when humans apply rotational deformations, risking crossings of the laser safety fences. In contrast, the mould has a simple, slightly concave shape with few collision points and no obstructions for the operator. At the same time, the ply is rectangular with good isotropic behaviour, as shown in Fig. 6(a).

In UC2, the route from the picking table to the mould is straightforward, with few obstacles. However, the mould is more complex, see Fig. 6(b), featuring higher dimensions and a broad concave shape, which increases the risk of collision between the robot gripper and the mould during placement. Additionally, the mould restricts the operator's visual access, and the manipulated ply has a complex shape and less isotropic behaviour than UC1, making accurate positioning difficult.

4.1. Experimental setup

The experimental setups used for the three use cases were the same. It comprises a heavy payload robot ABB IRB6700, a custom-made vacuum gripper developed within the DrapeBot project [37]; the gripper is equipped with up to 24 suction units able to pick the fabric-like material from the table, see Fig. 8. Each suction unit is independent and can move along the vertical axis with a stroke of 250 mm. One Azure Kinect RGB-D camera is on the gripper to detect the ply and estimate its deformation status. The gripper provides a User Interface (UI) screen with information for the user as the distance from the target position and direction.

[2] for the cases analysed, this method works well enough. Despite this, drift may appear, causing instability. A possible way to mitigate it is to clip the maximum value of $\hat{x}_{h,ref}$ to be not larger than a δ value with respect to the robot's trajectory.

The segmentation and deformation models have been trained following [40]. The dataset used to train both models comprises depth images of 2 plies with different shapes. The dataset comprises a total of roughly 6000 deformation states of the plies and a total of 60000 depth images. The dataset collection and labelling were performed autonomously without human intervention and required about 3 h. The segmentation and deformation models run on a dedicated PC with a Nvidia RTX 3060 GPU at approximately 30 Hz, the maximum frame rate of the Azure Kinect. On every use case, as a set of gains to convert deformations into wrenches, was experimentally chosen. A single set of gains is used for all the plies and the operators within a use case. The control architecture runs on a PC with Ubuntu 20.04 with a preemptive soft-real-time kernel, and it has been implemented in ROS [47]. The robot communication was at 4 ms, using ABB EGM protocol.

4.2. UC1, UC2 and UC3 experimental protocols

The cell layout used for the three use cases was similar; changes were made only on the mould and the picking table position, while the layout of the other components was identical. Considering the UC1 and the UC2 several users were involved to perform a human–robot collaborative transport. The transport consists of picking the carbon fibre ply from the picking table and placing it in the final position in the mould. The ply is picked from one side by the robot and on the opposite side by the human. Using the collaborative transport framework, each user performed the collaborative transport using the RA algorithm and with a Manual Guidance (MG) controller based on an admittance control algorithm that takes the delta deformation converted into virtual force as input, see Section 3.3. It is worth noting that the goal of the experimental part was to demonstrate the effectiveness of the proposed method on a concrete industrial use case and compare it with the current robotic state-of-the-art for solving these applications. The MG controller allows the robot to follow human intentions, minimising the deformation error from the deformation setpoint. Using the MG, the user has to guide the robot to the final position using the information provided by the UI installed on the gripper. The MG controller does not support the user in guiding the robot precisely to the final position. The deformation estimation pipeline was identical for both controllers, and the user had to drive the robot by applying deformation directly on the ply following the direction of the movement.

In the case of UC1, the controller was tested with three users, while in UC2, the controller was tested with four users. Each user did at least six trials (three with RA algorithm and three with the MG controller). A task is considered failed if the robot stops due to violating the operative robot workspace defined in the robot controller or if the operator cannot complete the task in 200 s. Each subject is let to practice with the controller before collecting data. During the task execution, the subject knows which control mode is active, either MG or RA. The subjects involved in the experiments differed from UC1 and UC2, and they already had experience in robotics usage (*i.e.,* medium-high robotic knowledge). The nominal collaborative trajectory used as a reference during the RA is computed using an RRT algorithm modified to include human walking speed and a maximum robot TCP speed set to 250 mm/s [48]. Motion planner development was not a topic of this research, and a third-party library was used for the experiments.

In UC3 the setup described in Section 4.1 was used to compare manual transport and draping with human–robot collaborative transport in a company's production facility. Without robotic experience, three personnel participated in producing a boat propeller, which involves 70 plies of materials like carbon fibre and fibreglass, see Fig. 7. The production process UC3 includes transporting plies from a picking table to the mould, draping them, and impregnating them with resin (repeated for all 70 plies). After placing all the plies in the mould, a vacuum foil was placed, and the curing process concluded the production of the part. Two different tests have been conducted: (i) manual production by two operators and (ii) collaborative transport using a robot for 38 of the

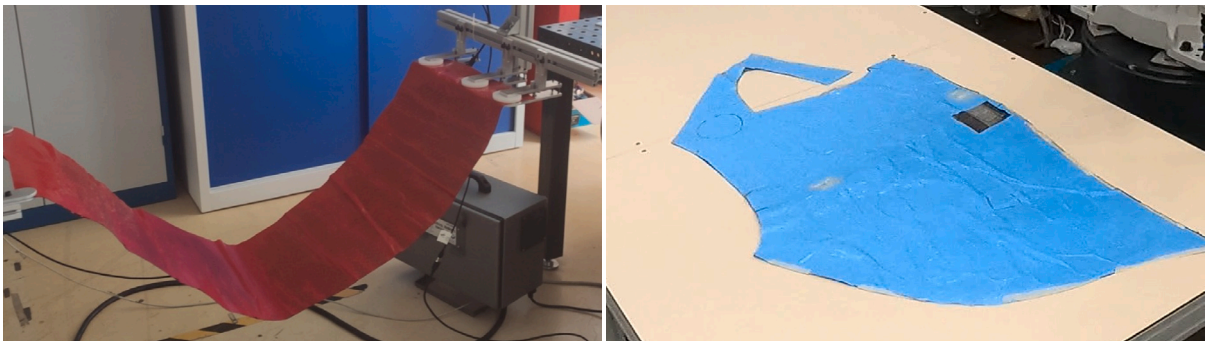

(a) (b)

Fig. 6. Plies used in the UC1 (a) and UC2 (b).

Fig. 7. UC3: Mould for the boat propeller production.

70 plies. The human followed the robot's trajectory without assistive algorithms for plies 1 to 9. Between plies 10 and 37, the human–robot collaboration involved a dynamic leadership exchange using the RA algorithm.

5. Human–robot collaborative transportation evaluation

This section presents the metrics used to evaluate the effectiveness of the proposed method on use cases UC1 and UC2. The RA algorithms were compared with a state-of-the-art MG method, showing performance improvements. Indices I1 and I5 were applied only to UC1. The I3, I4 and I6 were applied to UC1 and UC2, while I2 only to UC2. In cases where the index was not applied to both use cases, the rationale is reported after describing the index results.

Results are analysed and discussed. Statistical significance tests aid comparison between distributions. Specifically, the Mann–Whitney U Test (Wilcoxon Rank Sum Test) tests the mean value, and the Bartlett Test tests the variance. The significance level α for both tests is set to 0.05.

5.1. I_1 — Transport reliability

The transport reliability index I_1 is designed to count the number of trials necessary to complete a task three times, comparing the RA algorithm and the standard MG controller. Specifically, it is measured as three divided by the number of trials n_t required to reach three times the target position as

$$I_1 = \frac{3}{n_t}. \tag{6}$$

The transport is completed once the robot TCP enters a predefined tolerance of the final target position. The tolerance is defined as the sphere with a radius of 30 mm and centred in the final target position.

Table 1
UC1 I_1 The transport reliability index for the three users and the global using the two controllers computed using Eq. (6).

	MG	RA
usr1	100%	100%
usr2	75%	100%
usr3	60%	100%
Total	75%	100%

#UC1 Table 1 shows results relative to the transport reliability index I_1. Using MG algorithm, not all the users completed the task successfully in each trial. This is mainly because leading the robot far from the picking position after picking up the ply was complex; the gripper dimensions had to rotate by more than 90°. Such a rotation applies around the grasping point of the ply, located on one side of the gripper. Therefore, even a slight rotation around that point causes a significant motion at the rear of the gripper. The grasping point is close to a wall, making it extremely complex to move the robot. In the failure cases, the gripper hit the virtual safety fences to prevent the robot from colliding with the wall, and the task stopped. On the contrary, in the RA case, when the gripper approaches the wall (*i.e.,* the virtual safety fences), the robot knows the risk of a collision. It controls the human to recover the pre-computed safe and collision-free nominal trajectory. In this way, it was possible to avoid hitting the safety, and 100% of trials succeeded.

5.2. I_2 — Success rate

The success rate index I_2 computes the number of trials completed over the number of total trials, comparing RA and standard MG. The success rate I_2 is defined as

$$I_2 = \frac{n_s}{n_t}, \tag{7}$$

where n_s is the number of trials completed over the total trials n_t executed. The transport is completed once the robot TCP enters a predefined tolerance of the final target position. I_2 was computed with three different tolerances, so the spheres had a 300 mm, 150 mm, and 30 mm radius.

Two indices, I_1 and I_2 have been developed to take into account the peculiarity of each use case, *i.e.,* I_1 is applied to UC1 and I_2 is

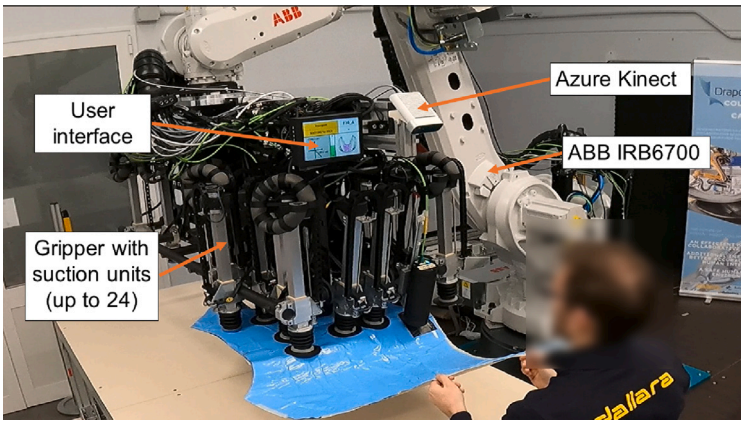

Fig. 8. The experimental setup used for UC1 and UC2.

Table 2
UC2 I_2 Success rate at reaching various distance tolerance, computed using Eq. (7).

Distance [m]	MG	RA
0.5	11/12	12/12
0.3	11/12	12/12
0.15	9/12	12/12
0.03	0/12	12/12

applied to UC2, since UC2 features a complex mould that imposes numerous constraints and limits the ability to reach the final target position. Consequently, achieving the desired tolerance with the robot's TCP is challenging, especially when employing the MG algorithm. As a result, the application of I_1 yields poor results with MG. Introducing I_2 facilitates a deeper and more equitable comparison between MG and RA, even if MG provided poorer results than RA.

#UC2 Table 2 shows the success rate at reaching various distances from the target in UC2.

The RA framework allowed all users to achieve a 100% success rate. Meanwhile, various failures occurred with the baseline MG framework. Specifically, in one case, a user immediately exceeded the robot's workspace since the picking table was close to the edge of the robot's workspace. Only in nine cases, the human was able to move the ply close to the target position (distance less or equal to 0.15 m); in the two remaining cases, the user was stopped after not being able to reach the target position within the time limit given for the experiment. Finally, no user could perform the accurate positioning (*i.e.,* distance less or equal to 0.03 m) with the MG control. Indeed, due to the size of the robotic application, it is extremely hard to command the robot accurately, and the required positioning accuracy is comparable with the precision of the deformation estimation. All the users were stopped after exceeding the maximum allowed time.

5.3. I_3 — Time to enter in tolerance

The index measures the time T required to reach the target position within a tolerance ϵ. To evaluate the effect of the control strategy for the two main sub-tasks of the collaborative transport, navigating to the target position and accurate positioning, multiple tolerance thresholds had been studied $\epsilon = [0.5\text{ m}, 0.3\text{ m}, 0.15\text{ m}, 0.03\text{ m}]$. Specifically, higher tolerances highlight the system's effectiveness in navigating toward the final target position in complex environments. Meanwhile, lower tolerance highlights the effectiveness in the final accurate positioning. The index is normalised over the nominal trajectory time T_n computed by the motion planner to allow comparison between the two use cases. I_3 is defined as

$$I_3 = \frac{T}{T_n}. \tag{8}$$

#UC1 and **#UC2** Fig. 9 shows the required normalised time to reach a certain distance from the target position, *i.e.,* distance tolerance, with the RA control strategy and the baseline MG. Four different distance tolerances are studied to investigate whether the RA strategy is helpful only in the final accurate positioning or in executing the trajectory.

The RA strategy allows statistically significant decreases in the mean and variance of the required time at all distance tolerances, particularly in the final accurate positioning where the tolerance is set to 30 mm. The statistical significance is verified for the cases UC1 and UC2; details are in the caption of Fig. 9. In UC2, as described in Table 2, no user could perform the final accurate positioning with the baseline MG. In UC1, the time reduction is stable across the various distance tolerances, highlighting that the most challenging part was the initial collaborative trajectories close to obstacles at the edge of the robot's workspace. Instead, in UC2, the reduction of time increases as the distance tolerance decreases, highlighting that providing precise commands to the robot for the final accurate positioning was the most challenging part of the collaborative task. The required time reduction is substantial in performing the first part of the trajectory and the final accurate positioning.

5.4. I_4 — Distance travelled

It compares the distance travelled with the nominal trajectory computed by the motion planner, the MG algorithm, and the RA algorithm. The I_4 is defined as the integral of the norm of the robot's instantaneous Cartesian speed, v

$$I_4 = \int_{T_{start}}^{T_{stop}} v\,dt. \tag{9}$$

#UC1 and **#UC2** Fig. 10 compares the distance travelled with RA, MG, and the baseline trajectory computed by the motion planner (MP) in the two use cases. In UC1, there is no significant difference between the two distributions in mean value ($p = 0.67$); meanwhile, there is a statistical difference in the variance ($p = 0.0079$). Reducing the variance value from MG to RA suggests that the RA framework helps humans perform complex manoeuvres close to obstacles, allowing more efficient trajectories. In UC2, there is no significant difference between the two distributions in mean value ($p = 0.63$) and variance ($p = 0.80$). It can easily explained by looking at the α value distribution in Fig. 15. Indeed, the trajectory for collaborative transport in UC2 is farther away from obstacles or workspace boundaries than UC1, as described in Section 4. Therefore, based on the designed arbitration law, humans are in charge most of the time, and the robot's behaviour is very similar to pure manual guidance, except for the human target estimation.

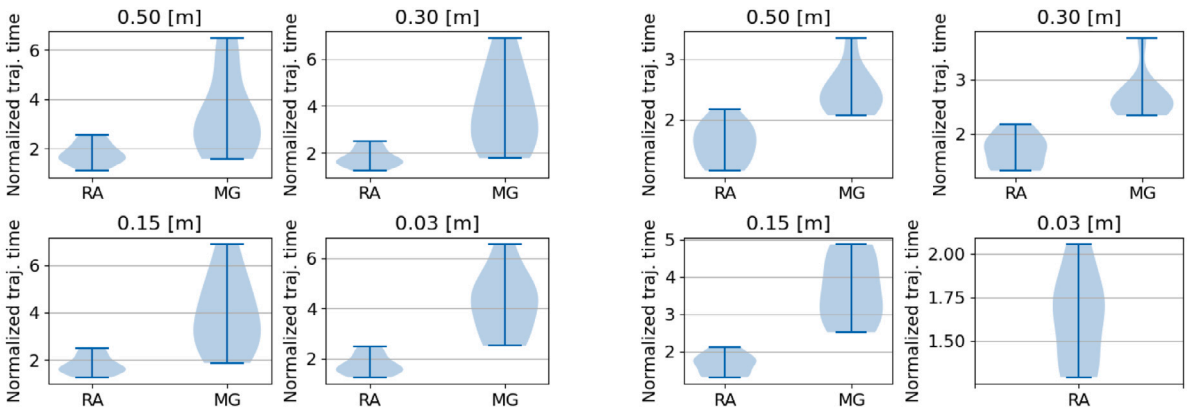

Fig. 9. I_3, the normalised time required to reach various target distances in both use cases UC1 (a) and UC2 (b) computed using Eq. (8). Specifically, for UC1, the p values are: Rank sum [0.00034, 0.00034, 0.00034, 0.00034] and Bartlett [0.017, 0.0014, 0.00061, 0.00033]; and for UC2: Rank sum [0.00081, 0.00077, 0.037] and Bartlett [0.0025, 0.00077, 2.25e−07].

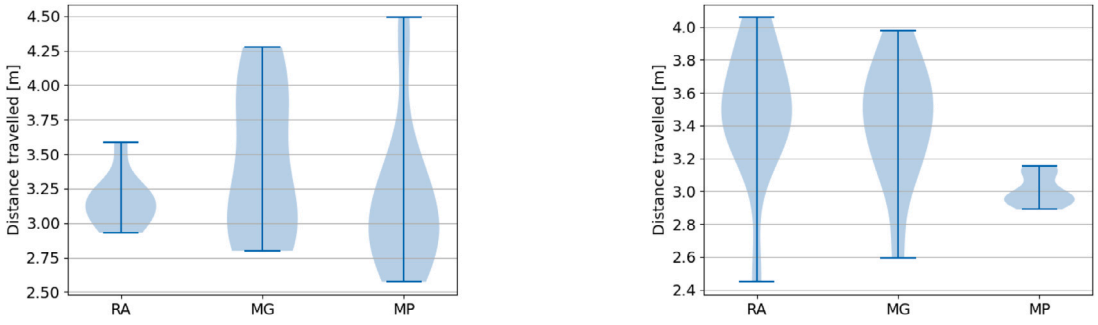

Fig. 10. I_4, comparison of the distribution of the distance travelled in UC1 (a) and UC2 (b) between RA, MG and MP. The index I_4 was computed using (9).

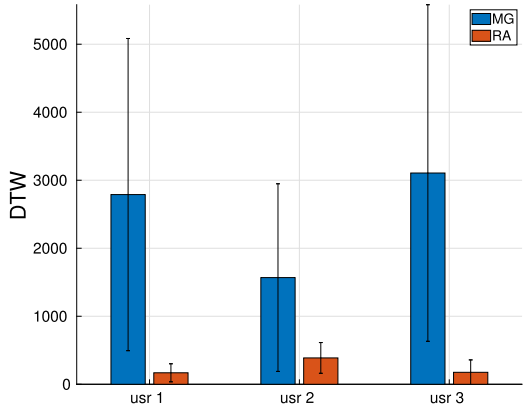

Fig. 11. I_5, DTW computed for UC1.

5.5. I_5 — *Dynamic time warping*

It measures how much the executed trajectory deviates from the nominal. For this purpose, the Dynamic Time Warping (DTW) was computed as in [49]. The DTW provides information about the geometrical distance between two trajectories without considering the time and possible time shifts between the two trajectories. It is helpful to see how well the cooperative trajectory executed tracks the original path. Indeed, following the nominal path can represent a great advantage if the trajectory is computed to comply with ergonomic constraints. In this case, the RA algorithm can also help humans work in ergonomic conditions that might be lost if humans guide robots. I_5 was computed only for UC1 because the cell layout (see the use case description in Section 4) imposes to the user more complex movements, bringing a different trajectory execution from the nominal one; these working conditions highlight the differences of DTW between the two control algorithms (*i.e.,* RA and MG). In the case of UC2, the layout allows the user to perform trajectories closer to the nominal one, so comparing DTWs is less relevant between the two controllers.

#UC1 Fig. 11 presents the DTW index. The lower the DTW value is, the more similar the two trajectories are. This shows that, in the RA case, the executed trajectory is more similar to the nominal one than the MG. In general, it is not fundamental that the executed and the planned trajectories are similar. Despite this, it can present some advantages. Consider a human-aware, ergonomic motion planner. In this case, it is very useful that the human follows the trajectory which is planned to be ergonomic. This can avoid long-term injuries due to wrong postures and working conditions. Moreover, consider an optimal motion planner: the closer the actual trajectory is to the planned one, the closer it is to optimality. This can improve cycle times if the trajectory is computed with that objective. Then, consider that some areas in the cell might be unsafe for working. The motion planner can plan a trajectory to avoid such areas. The closer the actual trajectory is, the safer it is. This last example happens in the proposed UC1 scenario when the robots avoid the human from hitting the safety fences by recovering their nominal trajectory.

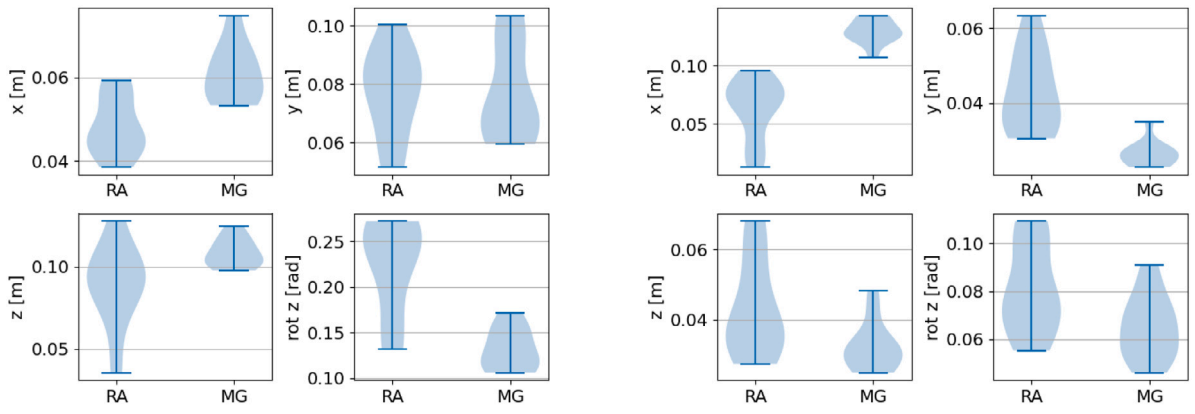

Fig. 12. I_6, deformation effort in UC1 (a) and UC2 (b) computed using (10).

5.6. I_6 — Deformation effort

The objective of the deformation effort is to study whether, thanks to the human target estimation, the RA strategy allows for a reduction in the amount of human input to command the robot. Therefore, we can consider the deformation effort as a proxy of the human effort. We define the deformation effort as the integral of the delta deformation Δd during the collaborative transportation normalised over the trajectory duration. In the RA strategy, the trajectory duration is limited only to the time the human is in charge, *i.e.*, $\alpha > 0.5$, and is denoted as T_α. Indeed, the estimated deformation when the robot is in charge does not represent commands given by the human; it is simply the robot pulling the human away from a dangerous situation or to the final target. The index I_6 is defined as

$$I_6 = \int_{T_{start}}^{T_{end}} \frac{|\Delta d|}{T_\alpha} dt \,. \tag{10}$$

#UC1 and **#UC2** Fig. 12 compares the distributions of the deformation effort between the RA and MG in both use cases. Except for the deformation effort along the x-axis, we cannot affirm that the RA strategy and the human target estimation allow reducing the number of inputs the human provides. At the same time, it appears to be increasing the deformation effort. However, such a result needs to be contextualised. First, the deformation efforts between RA and MG are generally similar, but the collaborative transport with the RA strategy is faster. Therefore, we can deduce that the proposed approach increases productivity without increasing the required human effort. Such a result could easily be seen in the non-normalised deformation effort. Second, the human target estimation described in (5) essentially integrates and amplifies the estimated deformation; thus, a minimum amount of deformation is necessary. Finally, it is also possible that the human operator adapts to the robot's speed. Specifically, in the MG case, once the operator notices that the robot is much slower than desired, he slows down to match the robot's speed, reducing the applied deformations.

5.7. Notes on the role arbitration results

The results in Figs. 13 and 14 represent a single test for UC1, the most significant case due to its complex collaborative transport environment. While UC2 yields similar conclusions, Fig. 13 illustrates the arbitration parameter α during collaborative transportation. Initially, when the pick position is near the safety fence, α is less than one as the human is assisted in moving away from the obstacle until α reaches one. As the human guides the robot, it approaches the safety fences, reducing collision distance around second 13. After this, the robot slowly commands the task. When the d_{trg} falls below d_o, the robot gains task control, and α drops to zero around second 33, allowing it to precisely reach the target position x_{trg}.

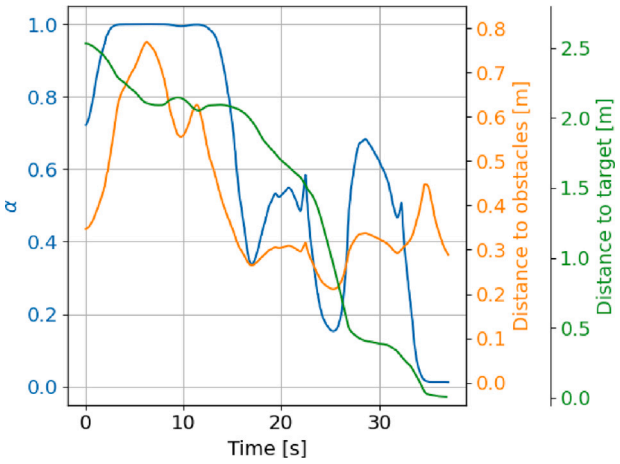

Fig. 13. Examples of the behaviour of the arbitration law, α, in the UC1 w.r.t. the distance from objects and the distance from the target.

Fig. 14 illustrates the nominal and actual trajectories based on a single test for UC1 (the same described above). Initially, the human leads the robot from the picking table (refer to Fig. 5(a)), resulting in significant differences between the two trajectories. The motion planner generates a trajectory (red line) that may be uncomfortable for humans due to its steep ascent before descending. Consequently, the operator modifies it to create a more reasonable trajectory (green line) that lowers the robot for user comfort. The robot takes control toward the end, and the two trajectories converge at the final point.

Fig. 15 shows the α value distribution for tests done on UC1 and UC2. Results indicate that in UC2, the operator leads most of the time ($\alpha \in [0.5-1]$) due to a more straightforward layout and fewer obstacles. In contrast, UC1 shows robots taking control ($\alpha \in [0-0.5]$) during the collaborative task to avoid collisions, resulting in less time for the operator to lead than UC2.

6. Manual vs human–robot collaborative transport (UC3)

This section analyses the results achieved during the production of a boat propeller, comparing the manual transport with the human–robot collaborative transport and draping. The experimental protocol followed was presented in Section 4.2. Examples of manual and human–robot collaborative transports are in Fig. 16.

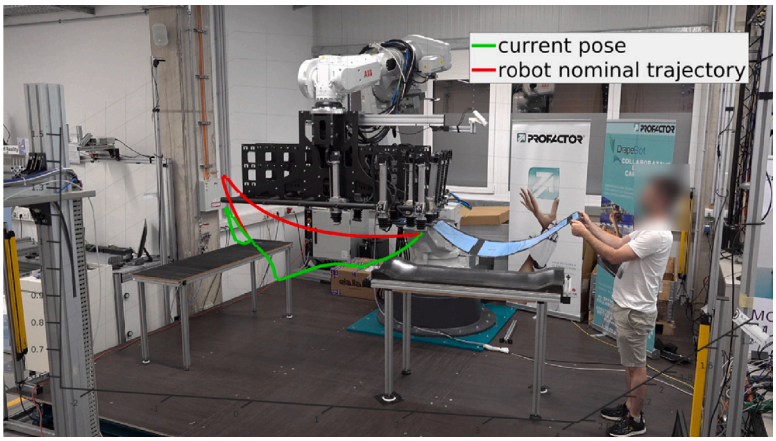

Fig. 14. The nominal (red line) and real (green line) robot trajectories projected in the robotic cell with the layout of UC1. (For interpretation of the references to colour in this figure legend, the reader is referred to the web version of this article.)

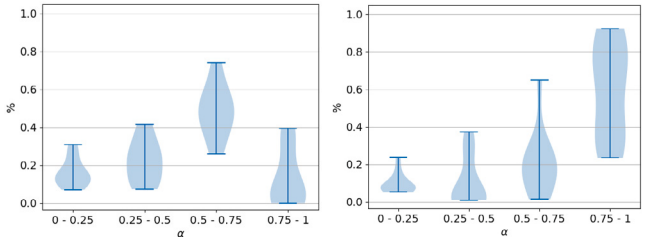

Fig. 15. Distribution of role allocation in the two use cases: (a) shows UC1 results, (b) shows UC2 results. Distributions prove that the role of arbitration law allows humans to be in charge most of the time, *i.e.,* $\alpha \in [0.5 - 1]$.

In UC3 the layout of the production cell was identical for both experiments, with video recordings taken. During the human–robot collaborative transport, the transport of three plies that failed were excluded from the analysis. The failures were due to wrong usage of the setup or a grasping issue by the robot.

The primary comparison factor was execution time. For manual transport, execution time T_m was measured from ply picking to the end of draping. For human–robot collaborative transport, execution time T_{hrc} was measured from when the robot was ready to move the ply until the operators completed the draping process. Looking at the results presented in Fig. 17, the manual transport brought always to faster transport and draping. On the contrary, using the robot allows for lower variability and a higher repeatability in cycle time. The presence of the assistive algorithm (ply 10–37) does not increase the time to complete the task compared to the transport where the operator was utterly passive (ply 1–9). Using the robot increased system complexity, leading to issues like ply grasping that can cause delays. However, it offers more repeatable and precise ply placement in the mould since the ply can be identified on the picking table by a vision system, in the specific case with an accuracy ±2 mm, and the accuracy of the robot in use is well below a millimetre. Under the assumption that the ply does not slide on the gripper during transport, it can be reasonably stated that the theoretical accuracy of the robotic system is higher than that of the human one during the placement of the ply. At the same time, the precision of the manual placement relies on the operator's experience and expertise, as well as the mould shape, while the robot usage is independent of these factors. Unfortunately, the shape of the part produced in the experiment prevented accurate measurement of its geometrical error. Currently, an expert operator visually inspects the component, and the propellers produced by both methods were comparable in manufacturing quality.

In addition to the operator engaged in transportation, a second operator impregnated the ply during robot operations, while a third operator supervised for safety ready to stop the robot in case of emergency. The presence of the third operator was motivated only by safety reasons, and no direct involvement in the production tasks was foreseen. The robot's TCP velocity was limited to 250 mm/s for safety. The presence of two operators is the standard for manual process. Their time occupancy is respectively 93% and 85%. These values decrease to 58% and 60% when using the robot for transport. Considering that the robot can also be used to automate other parts of the process, such as resin impregnation, the presence of the second operator can be avoided. The experimental robotic setup costs approximately ≈ 200k euros, with industrial-ready systems potentially higher in cost but offering benefits like improved accuracy, repeatability, and product traceability.

7. Conclusions and future works

This paper explores using RA to dynamically shift leadership between humans and robots while transporting large planar deformable objects collaboratively. It demonstrates this approach in two industrial cases, showing that the RA mechanism improves performance compared to state-of-the-art techniques, with higher success rates and reduced execution times. Comparisons with a standard MG control algorithm indicate that RA control outperforms MG control. Further improvements can be achieved by combining the RA algorithm with an optimal, human-aware motion planner for safer working conditions. The study compares RA to manual processes in boat propeller production, noting that while RA leads to longer production times, it offers greater repeatability and potentially workforce reduction. Future work will focus on developing a new motion planner to enhance execution speed and safety. The same approach will also be implemented on an Industrial Mobile Manipulator (IMM) to increase the system flexibility, allowing the transportation of planar deformable objects in a wider workspace.

CRediT authorship contribution statement

Enrico Villagrossi: Writing – review & editing, Writing – original draft, Supervision, Resources, Project administration, Methodology, Conceptualization. **Paolo Franceschi:** Writing – review & editing, Validation, Software, Methodology, Investigation, Data curation, Conceptualization. **Giorgio Nicola:** Writing – review & editing, Validation, Software, Methodology, Investigation, Data curation. **Nicola Pedrocchi:** Writing – review & editing, Supervision, Resources, Project administration, Funding acquisition, Conceptualization.

(a) (b)

Fig. 16. Production of a boat propeller (UC3): (a) reports one operator while making the manual transport of the ply from the picking table to the mould with the second operator giving support for the final placement in the mould and the impregnation, (b) reports the human–robot collaborative transport of the ply from the picking table to the mould performed by a single operator, while the second is waiting for the impregnation of the ply.

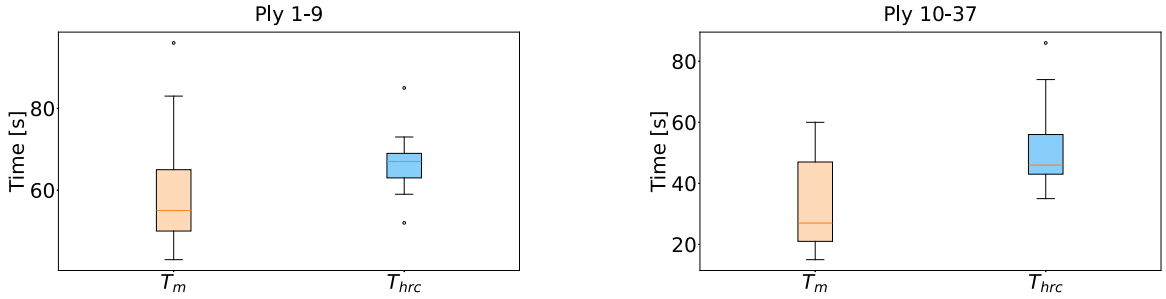

(a) (b)

Fig. 17. Results of experiments of UC3 for boat propeller production. (a) reports the boxplot of the time spent on the manual transport and draping T_m and the time spent for the human–robot collaborative transport and draping T_{hrc} for the plies from 1 to 9. In this case, the human–robot collaborative transport did not use the RA algorithm, but the operator was passively following the robot, executing a precomputed trajectory. (b) reports the boxplot of the time spent on the manual transport and draping T_m and the time spent for the human–robot collaborative transport and draping T_{hrc} for the plies from 10 to 37. In this case, the RA algorithm was active, and the role of the leader was arbitrated between the operator and the robot.

Declaration of competing interest

The authors declare that they have no known competing financial interests or personal relationships that could have appeared to influence the work reported in this paper.

Acknowledgements

This work has been funded by the European Union's Horizon 2020 research and innovation program under grant agreement No 101006732, "DrapeBot – A European Project developing collaborative draping of carbon fiber parts". The authors thank Matteo Casubolo from Dallara S.p.A, Simon Brunnmayr from Profactor GmbH, Thomas Elsken and Jakob Sabban from Baltico GmbH for their support during the experimental sessions. The authors also thank Silvia Menghini from CNR for the administrative management of DrapeBot.

Appendix

Control architecture

In this Appendix, the control architecture that was briefly introduced in Fig. 2 is detailed. Fig. 18 depicts the detailed control scheme developed in this work. Details on the GT modelling of the pHRI were originally proposed in [7].

Differential non-cooperative game theoretic interaction

In the non-cooperative case, the human and the robot aim to minimise their cost functions, subject to the other influences which are given by

$$J_{i,nc} = \int_0^\infty \left[(z - z_{ref,i})^T Q_i (z - z_{ref,i}) + u_i^T R_i u_i + u_j^T R_{i,j} u_j \right] dt \tag{11}$$

with pedices $i, j = \{h, r\}$ denoting human and robot, reciprocally. Where $z_{ref,i}$ are the human and robot reference targets, Q_i weight matrices on the state, R_i weight matrices on the player's control input, and $R_{h,i}$ weight matrices on the opponents' control input.

The non-cooperative differential game problem can be summarised as

$$\begin{aligned} &\min_{u_h} J_h(z, u_h, u_r) \\ &\min_{u_r} J_r(z, u_h, u_r) \\ &s.t.\ \dot{z} = Az + B_h u_h + B_r u_r \\ &z(t_0) = z_0 \end{aligned} \tag{12}$$

The Nash equilibrium is defined as

$$\begin{aligned} J_h(z, u_h^*, u_r^*) \leq J_h(z, u_h^*, u_r) \\ J_r(z, u_h^*, u_r^*) \leq J_r(z, u_h, u_r^*) \end{aligned} \tag{13}$$

and the control actions u_h and u_r are the Nash equilibrium policies. In the case of linear systems and quadratic cost functions, the control policies of the players are computed as

$$u_h = -K_{h,nc} (z - z_{ref,h}) \tag{14}$$

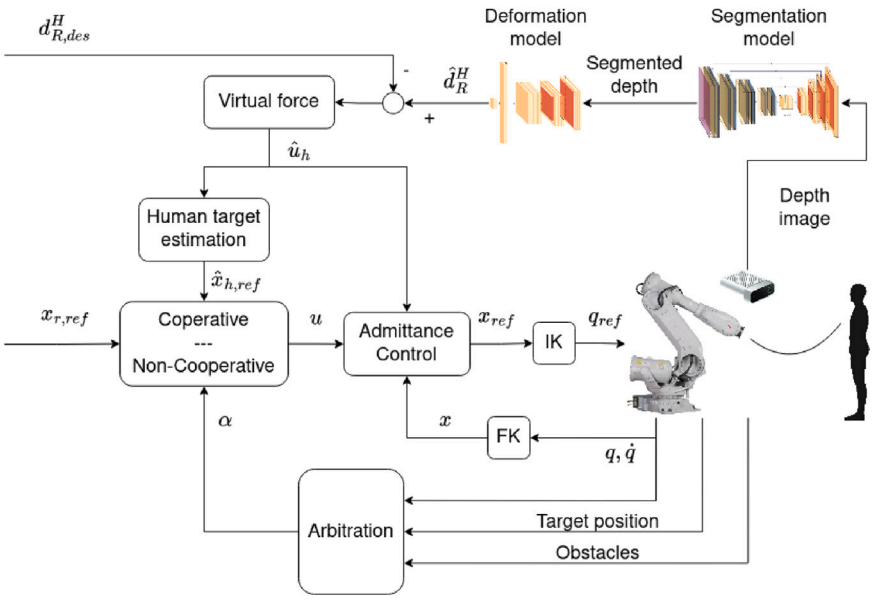

Fig. 18. The detailed control framework implemented for the human–robot collaborative transport.

and

$$u_r = -K_{r,nc}\,(z - z_{ref,r}) \tag{15}$$

The matrices $K_{h,nc}$ and $K_{r,nc}$ are the full-state feedback matrices, computed as $K_{h,nc} = R_h^{-1} B_h^T P_h$ and $K_{r,nc} = R_r^{-1} B_r^T P_r$, where P_h and P_r are solutions of coupled Riccati equations. For simplicity, define with $S_i = B_i R_{i,i} B_i^T$ and $S_{i,j} = B_i R_{i,i}^{-1} R_{j,i} R_{i,i}^{-1} B_i^T$, with $i = \{h,\ r\}$. The two coupled Riccati equations are

$$0 = (A - S_j P_j)^T P_i + P_i (A - S_j P_j)^T - P_i S_i P_i + P_j S_{j,i} P_j + Q_i \tag{16}$$

Differential cooperative game theoretic interaction

The Cooperative formulation of the problem allows agreement between the players to define a shared objective and work together toward it. In a cooperative framework, the human and the robot can be seen as two agents, each one to minimise a quadratic cost function, defined as

$$J_{i,c} = \int_0^\infty \big[\,(z - z_{ref,i})^T\, Q_{i,i}\,(z - z_{ref,i}) + (z - z_{ref,j})^T\, Q_{i,j}\,(z - z_{ref,j}) + u_i^T\, R_i\, u_i\,\big]\ dt \tag{17}$$

with i, j as above, where $J_{i,c}$ are the costs that the human and the robot incur, $Q_{i,i}, Q_{i,j}$ matrices that weight the state and references and R_i weights on the control input.

By cooperating, a shared objective is defined as

$$J_c = \alpha\, J_h + (1 - \alpha)\, J_r = \int_0^\infty \left(\tilde{z}^T\, Q_c\, \tilde{z} + u^T\, R_c\, u\right)\ dt \tag{18}$$

with $\tilde{z} = z - z_{ref}$, where z_{ref}, Q_c and R_c must be defined, as discussed in [50].

The Linear Quadratic Differential Game problem can be finally formulated as a classical LQR problem:

$$\begin{aligned} \min_u J_c &= \int_0^\infty \left(z^T\, Q_c\, z + u^T\, R_c\, u\right)\ dt \\ s.t.\ \dot{z} &= A\, z + B u \\ z(t_0) &= z_0 \end{aligned} \tag{19}$$

The problem in (19) has infinite solutions lying on the Pareto frontier, depending on the parameter α.

In an LQ-CGT framework, the control action u is defined as full-state feedback as

$$u = -K_{gt}\,\tilde{z} = -K_{gt}\,z + K_{gt}\,z_{ref} \tag{20}$$

with $K_{gt} = R_c^{-1} B^T P$ and matrix P solution of the Algebraic Riccati Equation (ARE)

$$0 = A^T P + P A^T - P B R_c^{-1} B^T P + Q_c$$

Note that $u = [u_h, u_r]^T$. Therefore, the human and robot control inputs can be extracted by slicing the vector of control inputs.

References

[1] Krishnan A, Yang X, Seth U, Jeyachandran JM, Ahn JY, Gardner R, et al. Data-driven ergonomic risk assessment of complex hand-intensive manufacturing processes. Commun Eng 2025;4(1). http://dx.doi.org/10.1038/s44172-025-00382-w.

[2] Khan WA, Anjum MU, Khan H, Hamza A, Jabbar H, Zafar T, et al. Application of robotic manipulation for carbon fiber reinforced polymers manufacturing—A survey. Compos Part C: Open Access 2024;15:100503. http://dx.doi.org/10.1016/j.jcomc.2024.100503.

[3] Franceschi P, Pedrocchi N, Beschi M. Adaptive impedance controller for human–robot arbitration based on cooperative differential game theory. In: 2022 international conference on robotics and automation. ICRA, 2022, p. 7881–7. http://dx.doi.org/10.1109/ICRA46639.2022.9811853.

[4] Dumora J, Geffard F, Bidard C, Brouillet T, Fraisse P. Experimental study on haptic communication of a human in a shared human–robot collaborative task. Int Conf Int Rob Syst 2012;5137–44. http://dx.doi.org/10.1109/IROS.2012.6385721.

[5] Jensen SW, Salmon JL, Killpack MD. Trends in haptic communication of human-human dyads: Toward natural human–robot Co-manipulation. Front Neurorobotics 2021;15. http://dx.doi.org/10.3389/fnbot.2021.626074.

[6] Nicola G, Villagrossi E, Pedrocchi N. Co-manipulation of soft-materials estimating deformation from depth images. Robot Comput-Integr Manuf 2024;85:102630. http://dx.doi.org/10.1016/j.rcim.2023.102630.

[7] Franceschi P, Pedrocchi N, Beschi M. Human–robot role arbitration via differential game theory. IEEE Trans Autom Sci Eng 2023;1–16. http://dx.doi.org/10.1109/TASE.2023.3320708.

[8] Makris S, Dietrich F, Kellens K, Hu SJ. Automated assembly of non-rigid objects. CIRP Ann 2023;72(2):513–39. http://dx.doi.org/10.1016/j.cirp.2023.05.003.

[9] Lee AX, Lu H, Gupta A, Levine S, Abbeel P. Learning force-based manipulation of deformable objects from multiple demonstrations. In: 2015 IEEE int conf on rob and aut. 2015, p. 177–84. http://dx.doi.org/10.1109/ICRA.2015.7138997.

[10] Li Y, Yue Y, Xu D, Grinspun E, Allen PK. Folding deformable objects using predictive simulation and trajectory optimization. In: Int conf on int rob and syst. IROS, 2015, p. 6000–6. http://dx.doi.org/10.1109/IROS.2015.7354231.

[11] Schuster A, Frommel C, Deden D, Brandt L, Eckardt M, Glück R, et al. Simulation based draping of dry carbon fibre textiles with cooperating robots. Procedia Manuf 2019;38:505–12. http://dx.doi.org/10.1016/j.promfg.2020.01.064, 29th International Conference on Flexible Automation and Intelligent Manufacturing, June 24-28, 2019.

[12] Kermenov R, Foix S, Borràs J, Castorani V, Longhi S, Bonci A. Automating the hand layup process: On the removal of protective films with collaborative robots. Robot Comput-Integr Manuf 2025;93:102899. http://dx.doi.org/10.1016/j.rcim.2024.102899.

[13] Gombo Y, Tiwari A, Safwat M, Chang H, Devasia S. Communication-free decentralized controller design for flexible object transport. IEEE/ASME Trans Mechatronics 2024;1–10. http://dx.doi.org/10.1109/TMECH.2024.3399120.

[14] Matsas E, Vosniakos G-C, Batras D. Prototyping proactive and adaptive techniques for human–robot collaboration in manufacturing using virtual reality. Robot Comput-Integr Manuf 2018;50:168–80. http://dx.doi.org/10.1016/j.rcim.2017.09.005.

[15] Papadopoulos G, Andronas D, Kampourakis E, Theodoropoulos N, Kotsaris PS, Makris S. On deformable object handling: Multi-tool end-effector for robotized manipulation and layup of fabrics and composites. Int J Adv Manuf Technol 2023;128:1675–87. http://dx.doi.org/10.1007/s00170-023-11914-z.

[16] De Schepper D, Schouterden G, Kellens K, Demeester E. Human-robot mobile co-manipulation of flexible objects by fusing wrench and skeleton tracking data. Int J Comput Integr Manuf 2022;36(1):30–50. http://dx.doi.org/10.1080/0951192X.2022.2081362, arXiv:10.1080/0951192X.2022.2081362.

[17] Lou S, Zhang Y, Tan R, Lv C. A human-cyber-physical system enabled sequential disassembly planning approach for a human–robot collaboration cell in industry 5.0. Robot Comput-Integr Manuf 2024;87:102706. http://dx.doi.org/10.1016/j.rcim.2023.102706.

[18] Franceschi P, Bussolan A, Pomponi V, Avram O, Baraldo S, Valente A. Human-robot collaborative transport personalization via dynamic movement primitives and velocity scaling. In: 2025 34th IEEE International Conference on Robot and Human Interactive Communication (RO-MAN). 2025, p. 1235–42. http://dx.doi.org/10.1109/RO-MAN63969.2025.11217816.

[19] Andronas D, Kokotinis G, Makris S. On modelling and handling of flexible materials: A review on digital twins and planning systems. Procedia CIRP 2021;97:447–52. http://dx.doi.org/10.1016/j.procir.2020.08.005, 8th CIRP Conference of Assembly Technology and Systems.

[20] De Schepper D, Moyaers B, Schouterden G, Kellens K, Demeester E. Towards robust human–robot mobile co-manipulation for tasks involving the handling of non-rigid materials using sensor-fused force-torque, and skeleton tracking data. Procedia CIRP 2021;97:325–30. http://dx.doi.org/10.1016/j.procir.2020.05.245, 8th CIRP Conference of Assembly Technology and Systems.

[21] Sirintuna D, Giammarino A, Ajoudani A. An object deformation-agnostic framework for human–robot collaborative transportation. IEEE Trans Autom Sci Eng 2024;21(2):1986–99. http://dx.doi.org/10.1109/TASE.2023.3259162.

[22] Sirintuna D, Giammarino A, Ajoudani A. Human–robot collaborative carrying of objects with unknown deformation characteristics. In: Int conf on int rob and syst. IROS, 2022, p. 10681–7. http://dx.doi.org/10.1109/IROS47612.2022.9981948.

[23] Bonci A, Di Biase A, Longhi S, Kermenov R. Human–robot Co-transport of flexible materials using deformation constraints. In: 2024 IEEE 29th international conference on emerging technologies and factory automation. ETFA, 2024, p. 1–7. http://dx.doi.org/10.1109/ETFA61755.2024.10711132.

[24] Kermenov R, Di Biase A, Pellicani I, Longhi S, Bonci A. Near time-optimal trajectories with ISO standard constraints for human–robot collaboration in fabric Co-transportation. Robotics 2025;14(2). http://dx.doi.org/10.3390/robotics14020010.

[25] Kruse D, Radke RJ, Wen JT. Human-robot collaborative handling of highly deformable materials. In: 2017 American control conference. ACC, 2017, p. 1511–6. http://dx.doi.org/10.23919/ACC.2017.7963167.

[26] Nicola G, Villagrossi E, Pedrocchi N. Human-robot co-manipulation of soft materials: Enable a robot manual guidance using a depth map feedback. In: 2022 31st IEEE international conference on robot and human interactive communication. RO-MAN, 2022, p. 498–504. http://dx.doi.org/10.1109/RO-MAN53752.2022.9900710.

[27] Mohebbi A. Human–robot interaction in rehabilitation and assistance: A review. Curr Robot Rep 2020;1:131–44. http://dx.doi.org/10.1007/s43154-020-00015-4.

[28] Casas J, Cespedes N, Múnera M, Cifuentes CA. Human-robot interaction for rehabilitation scenarios. In: Azar AT, editor. Control systems design of bio-robotics and bio-mechatronics with advanced applications. Academic Press; 2020, p. 1–31. http://dx.doi.org/10.1016/B978-0-12-817463-0.00001-0.

[29] Lawitzky M, Mörtl A, Hirche S. Load sharing in human–robot cooperative manipulation. In: 19th international symposium in robot and human interactive communication. 2010, p. 185–91. http://dx.doi.org/10.1109/ROMAN.2010.5598627.

[30] Bazzi D, Priora G, Zanchettin AM, Rocco P. RRT* and goal-driven variable admittance control for obstacle avoidance in manual guidance applications. IEEE Robot Autom Lett 2022;7(2):1920–7. http://dx.doi.org/10.1109/LRA.2022.3142887.

[31] Li Y, Tee KP, Chan WL, Yan R, Chua Y, Limbu DK. Continuous role adaptation for human–robot shared control. IEEE Trans Robot 2015;31(3):672–81. http://dx.doi.org/10.1109/TRO.2015.2419873.

[32] Bi W, Wu X, Liu Y, Li Z. Role adaptation and force, impedance learning for physical human–robot interaction. In: 2019 IEEE 4th international conference on advanced robotics and mechatronics. ICARM, 2019, p. 111–7. http://dx.doi.org/10.1109/ICARM.2019.8834320.

[33] Li Y, Tee KP, Yan R, Chan WL, Wu Y, Limbu DK. Adaptive optimal control for coordination in physical human–robot interaction. In: Int conf on int rob and syst. IROS, 2015, p. 20–5. http://dx.doi.org/10.1109/IROS.2015.7353109.

[34] Li Y, Tee KP, Yan R, Chan WL, Wu Y. A framework of human–robot coordination based on game theory and policy iteration. IEEE Trans Robot 2016;32(6):1408–18. http://dx.doi.org/10.1109/TRO.2016.2597322.

[35] Musić S, Hirche S. Haptic shared control for human–robot collaboration: A game-theoretical approach. IFAC-PapersOnLine 2020;53(2):10216–22. http://dx.doi.org/10.1016/j.ifacol.2020.12.2751, 21st IFAC World Congress.

[36] MERGING Consortium. Manipulation enhancement through robotic guidance and intelligent novel grippers (MERGING). 2019, URL http://www.merging-project.eu/.

[37] DrapeBot Consortium. DrapeBot — A European project developing collaborative draping of carbon fiber parts. 2021, URL https://www.drapebot.eu/.

[38] Makris S, Kampourakis E, Andronas D. On deformable object handling: Model-based motion planning for human–robot Co-manipulation. CIRP Ann 2022;71(1):29–32. http://dx.doi.org/10.1016/j.cirp.2022.04.048.

[39] Eitzinger C, Frommel C, Ghidoni S, Villagrossi E. System concept for human–robot collaborative draping. In: SAMPE europe conference. 2021, p. 7542–9.

[40] Nicola G, Mutti S, Villagrossi E, Pedrocchi N. Depth image-based deformation estimation of deformable objects for collaborative mobile transportation. In: 2023 32nd IEEE international conference on robot and human interactive communication. RO-MAN, 2023, p. 2658–64. http://dx.doi.org/10.1109/RO-MAN57019.2023.10309337.

[41] Franceschi P, Mutti S, Pedrocchi N. Optimal design of robotic work-cell through hierarchical manipulability maximization. Robot Comput-Integr Manuf 2022;78:102401.

[42] Cremer S, Das SK, Wijayasinghe IB, Popa DO, Lewis FL. Model-free online neuroadaptive controller with intent estimation for physical human–robot interaction. IEEE Trans Robot 2020;36(1):240–53. http://dx.doi.org/10.1109/TRO.2019.2946721.

[43] Li Y, Eden J, Carboni G, Burdet E. Improving tracking through human–robot sensory augmentation. IEEE Robot Autom Lett 2020;5(3):4399–406. http://dx.doi.org/10.1109/LRA.2020.2998715.

[44] Leica P, Roberti F, Monllor M, Toibero JM, Carelli R. Control of bidirectional physical human–robot interaction based on the human intention. Intell Serv Robot 2017;10(1):31–40. http://dx.doi.org/10.1007/s11370-016-0207-4.

[45] Franceschi P, Bertini F, Braghin F, Roveda L, Pedrocchi N, Beschi M. Learning human motion intention for pHRI assistive control. In: Int conf on int rob and syst. IROS, 2023, p. 7870–7. http://dx.doi.org/10.1109/IROS55552.2023.10342014.

[46] Franceschi P, Cassinelli D, Pedrocchi N, Beschi M, Rocco P. Design of an assistive controller for physical human–robot interaction based on cooperative game theory and human intention estimation. IEEE Trans Autom Sci Eng 2024.

[47] Stanford Artificial Intelligence Laboratory, et al. Robotic operating system. 2025, URL https://www.ros.org. [Accessed 15 October 2025].

[48] Gottardi A, Terreran M, Frommel C, Schoenheits M, Castaman N, Ghidoni S, et al. Dynamic human-aware task planner for human–robot collaboration in industrial scenario. In: 2023 European conference on mobile robots. ECMR, 2023, p. 1–8. http://dx.doi.org/10.1109/ECMR59166.2023.10256268.

[49] Müller M. Dynamic time warping. In: Information retrieval for music and motion. Berlin, Heidelberg: Springer Berlin Heidelberg; 2007, p. 69–84. http://dx.doi.org/10.1007/978-3-540-74048-3_4.

[50] Franceschi P, Beschi M, Pedrocchi N, Valente A. Modeling and analysis of pHRI with differential game theory. In: 2023 21st international conference on advanced robotics. ICAR, 2023, p. 277–84. http://dx.doi.org/10.1109/ICAR58858.2023.10406758.